11th International Conference on Fracture Mechanics of Concrete and Concrete Structures
FraMCoS-11
J. M. Chandra Kishen, A. Ramaswamy, S. Ray and R. Vidyasagar (Eds)
https://doi.org/10.21012/FC11.092382

RESIDUAL CAPACITY OF FATIGUE-PRONE REINFORCED CONCRETE STRUCTURES

BENARD M. ISOJEH[*] AND MOHAMMAD AFAGHI[†]

[*] Civil Engineering Department, Lassonde School of Engineering, York University, North York, Ontario, Canada
Bergeron Centre, North York, ON M3J 2S5, Canada
e-mail: bisojeh@yorku.ca

[†] Department of Structural Engineering, Norwegian University of Science and Technology, Trondheim, Norway
e-mail: mohammad.afaghi@ntnu.no

Key words: Damage, fracture, Residual capacity, irreversible fatigue strain

Abstract: Designing reinforced concrete structures susceptible to fatigue damage requires satisfying the fatigue limit state. Current codes' stress-life curve considerations are confined to the design stages and cannot be used to monitor evolving fatigue damage if the structure in service is subjected to severe environmental conditions or loads that are higher than the design values.

One significant observation in the area of fatigue damage is the scatter in results from various stress-life models. In addition, the use of S-N curves in areas of high local stresses exceeding stress-life curve limits does not necessarily mean global failure, especially if the structural stability is not affected.

Reports on collapsed wind turbines due to foundation failure often indicate wind farm shutdown periods to enable investigations. The lack of means to study damage evolution or observe residual capacity of such reinforced concrete structures often results in the recommendation to rehabilitate all the foundations in most cases; hence, incurring significant losses.

This report proposes an innovative approach that utilizes finite element analysis framework to predict the damage evolution and the residual capacity of reinforced concrete structures after a given number of fatigue loading cycles. The advantage of this approach stems from the fact that recorded wind loads and cycles from wind turbines can be read into the algorithm and the variations in loading amplitudes are considered in the analyses.
To verify the model's reliability, fatigue life and residual capacity estimations are conducted on reinforced concrete specimens that were tested under fatigue loading. The results obtained portrayed substantial correlation.

1 INTRODUCTION

Fatigue-prone structures, such as wind turbine foundations, are designed to prevent the development of fatigue damage by mitigating induced stresses. Various engineering codes propose stress-life equations and endurance limit stresses to ensure safe designs [1,2,3,4]. Some codes have resulted in conservative designs when loads and corresponding stresses are accurately estimated.

In practical scenarios, a fatigue-prone

structural element may be subjected to higher loads than initially designed, or environmental and chemical factors may reduce its fatigue load resistance capacity. Even if the original design were conservative, the structure could be undergoing fatigue damage due to reduced resistance capacity [5].

The paramount task is to verify the fatigue residual capacity of such structures to prevent catastrophic failures. This manuscript presents an approach to estimate the residual capacity and damage evolution of fatigue-prone structural elements. The method incorporates models for concrete damage and steel crack growth, derived from experimental data, into a finite element analysis framework. Each material model will be discussed in subsequent sections, and deformation evolution results from previous experiments will be compared with finite element analysis (FEA) results. Additionally, the estimation of the residual capacity of a test specimen after a given number of fatigue loading cycles will be made.

2 CONCRETE DAMAGE

Low concrete stress is generally not associated with fatigue damage. However, as concrete stresses increase, the potential for fatigue damage also rises. Numerous fatigue tests conducted under uniaxial and biaxial tension or compression have demonstrated fatigue damage in terms of the number of cycles to failure, irreversible strain accumulation, evolving temperature, and reductions in strength and stiffness, among other factors. Non-Destructive Testing (NDT) methods have also been utilized to assess fatigue damage evolution based on parameters like the velocity of sound [1,2].

This paper proposes a method to account for fatigue damage by considering the accumulated irreversible fatigue strain in tension and compression, as well as stiffness and strength reductions.

The irreversible fatigue strain and damage models for concrete used are given thus [6,7,8] (see Figure 1.0).

For concrete in compression,

$$\varepsilon_{d0} = \left(\frac{f_c' + (\sigma_{max}\, R)}{E}\right) - 0.3\, \varepsilon_c' \tag{1}$$

$$\varepsilon_{d1} = \frac{\sigma_{max}\, R}{E_{sec}} \tag{2}$$

$$\varepsilon_{c2}^{fat} = \varepsilon_{d0} + \varepsilon_{d1} \tag{3}$$

For concrete in tension,

$$\varepsilon_{c1}^{fat} = \frac{f_t' + (\sigma_{max}\, R)}{E} \tag{4}$$

$$\mathrm{E} = (1 - D)E_c \tag{5}$$

$$D = D_{cr}\, \mathrm{Exp}\left[s\left(\frac{\sigma_{max}}{f_c'} - u\right)\right] N^v \tag{6}$$

$$u = C_f\left(1 - \gamma_2 \log(\zeta N_f T)\right) \tag{7}$$

$$v = 0.434\, s\, C_f\left(\beta_2(1 - R)\right) \tag{8}$$

$$C_f = ab^{-\log f} + c \tag{9}$$

$$\beta_2 = 0.0661 - 0.0226R \tag{10}$$

where a, b and c are 0.249, 0.920 and 0.796 respectively, and f is the frequency of the fatigue loading. $\gamma_2 = 0.0247$. C_f accounts for the influence of loading frequency [8].

ζ is a dimensionless coefficient that is taken as 0.15 for sinusoidal waveform. f_c' is the compressive strength of concrete, f_t' is the tensile strength of concrete, σ_{max} is the maximum stress in concrete, σ_{min} is the minimum stress in concrete (equal to $\sigma_{max}R$).

E is the stiffness of concrete after fatigue degradation, ε_c' is the concrete strain corresponding to the peak stress in concrete, E_{sec} is the secant stiffness in concrete, N is the number of fatigue loading cycles, D_{cr} is taken as 0.4 for stiffness degradation and 0.35 for strength degradation. f is the frequency of loading, and s is a material parameter that can be estimated as:

for strength degradation,

$$s = 1851.9R^3 + 111.11R^2 + 460.85R + 350.16 \quad (11)$$

for stiffness degradation,

$$s = 259.26R^3 - 33.37R^2 + 66.02R + 39.86 \quad (12)$$

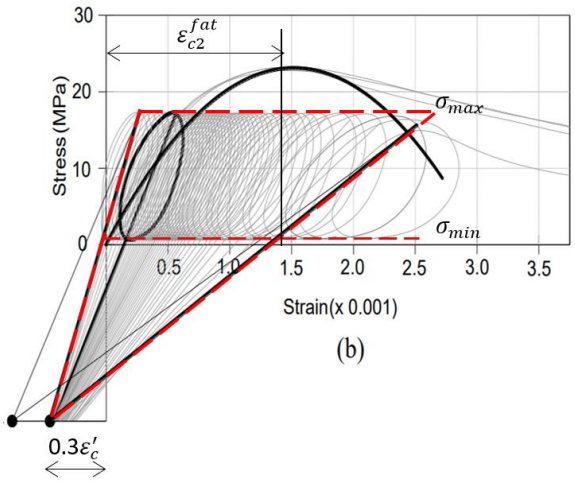

Figure 1.0: Fatigue degradation of concrete in compression (each hysteresis has an interval of 100 cycles)

3 REINFORCEMENT FRACTURE

Reinforcement passing through cracked concrete planes experiences higher stresses compared to regions embedded in the concrete. When subjected to fatigue loading, crack initiation may occur on the rebars, and the cracks may propagate until the remaining cross-sectional area of the rebars becomes unable to withstand tensile forces or bridge the cracked concrete. Consequently, the shear stress on the crack plane and the average tensile stresses between cracks vary as the reinforcement area reduces. Furthermore, the ongoing fatigue loading induces irreversible strains in the steel reinforcement [7].

To accurately capture these mechanisms, it is essential to account for the progressive crack growth in the reinforcement and the induced fatigue strains in the rebars. In this context, a strain-life fatigue model is employed to consider crack nucleation, while a fracture mechanics model is utilized to account for crack growth or rebar area reduction. The expressed models are as follows:

From Figure 2.0, the general static equilibrium equations (between cracks and at crack plane) for steel fiber concrete are given as [9,10,11]:

$$f_{c1} = \sum_i^n \rho_{si}\,(Z_0 f_{scri} - f_{si}).\,cos^2\theta_{ni} + (1 - \alpha_{avg}) f_f \sqrt{1 - D}\; cos\theta_f \quad (13)$$

$$v_{ci,cr} = \sum_i^n \rho_{si}\,(Z_0 f_{scri} - f_{si}).\,cos\theta_{ni}\; sin\theta_{ni} - (1 - \alpha_{avg}) f_f \sqrt{1 - D}\; sin\theta_f \quad (14)$$

D in Equations 13 and 14 corresponds to strength damage (Equation 6). $v_{ci,cr}$ is the shear stress on crack surface; f_{c1} is the principal tensile stress in concrete; ρ_{si} is the reinforcement ratio; f_{scri} is the local stress (at crack) in conventional reinforcement; f_{si} is the average stress in conventional reinforcement.

θ_{ni} is the angle between conventional reinforcement and normal to crack; α_{avg} is the coefficient to relate tensile stress at a crack due to steel fibers with average tensile stress; f_f is the tensile stress at the crack due to steel fibers; and θ_f is the angle between tensile stress direction due to steel fibers and principal tensile stress direction in concrete.

Equations 13 and 14 must be satisfied as specified in The Modified Compression Field Theory (MCFT) and The Disturbed Stress Field Theory (DSFT).

Equation 14 plays a crucial role in calculating the slip within a concrete crack plane and is also considered as a prestrain [9,10]. The consideration of this prestrain is presented in a subsequent section. The derivations of these equations can be found in references [9], [10], and [11].

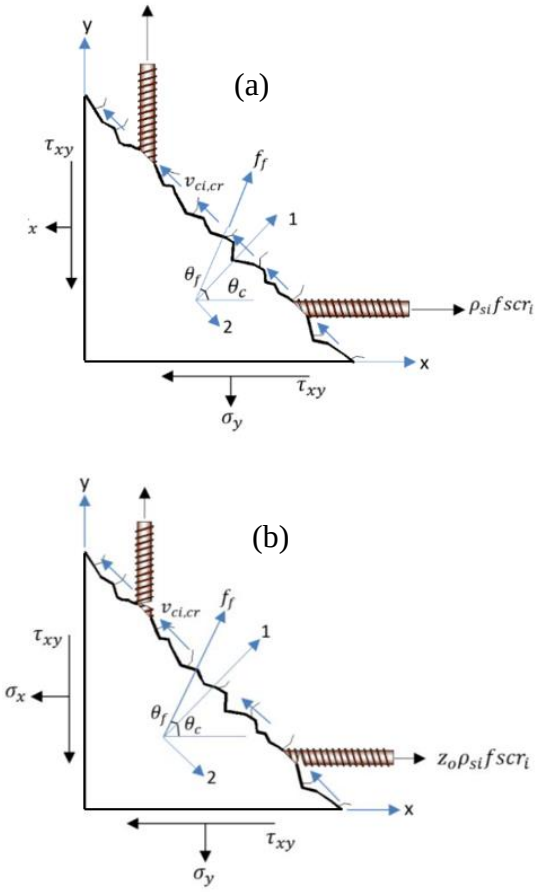

Figure 2.0: Equilibrium conditions along crack surface after reinforcement crack propagation (a) shows rebars traversing a concrete crack without crack growth. (b) show rebars with crack growth.

In Equations 13 and 14, Z_0 (reinforcement crack growth factor) is estimated as:

$$Z_0 = \frac{A_{res}}{A_0}$$

The residual area (A_{res}) of a reinforcing bar after crack propagation to a given number of cycles is obtained as:

$$A_{res} = A_0 - A(a_y) \quad (15)$$

$$A(a_y)k = \frac{\theta_r}{90}\pi r^2 - r sin\theta_r (2r - a_y) \quad (16)$$

$$\theta_r = cos^{-1}\left(\frac{r - a_y}{r}\right) \quad (17)$$

k is taken as 2.0.

The fractured surface area (A(a_y)) of a reinforcing bar can be approximated as depicted in Figure 3.0. The crack depth (ay) evolves from plastic nucleation or crack initiation until the point when the reserve capacity of the reinforcement at the crack is no longer adequate for tensile stress transfer [12]. As emphasized previously, a strain life model described in [13] is used to estimate the number of cycles that will result in plastic nucleation. The SWT model was implemented; however, the values for the constants used include:

b = -0.09, c = -0.56, $\varepsilon_f' = (0.32H'^2 - 487H' + 191000)/E_s$; $\sigma_f = 4.25H' + 225$ MPa, n' = b/c = 0.15, H' = ultimate strength of steel/345.

To estimate the crack depth (a_y) after a given number of cycles, Equation 18 [12] is utilized.

$$a_y = \left(\frac{a_i^{\alpha}}{1 - \left[N_{ij}\left(C.\alpha.\pi^{\frac{n}{2}}.Y^n.\Delta\sigma^n.a_i^{\alpha}\right)\right]}\right)^{\frac{1}{\alpha}} \quad (18)$$

where $\alpha = (n/2)\text{-}1$; $C = 2 \times 10^{-13}$; and $n = 3.0$, a_i and a_y are the previous and current crack depth for the interval of cycles considered (N_{ij}), respectively. Y is the shape factor, proposed in BS 7910 (1999) [14] as a function of the crack depth. The full equations may be found in [12 and 13].

A_0 is the cross-sectional area of the uncracked rebar. r is the reinforcing bar radius.

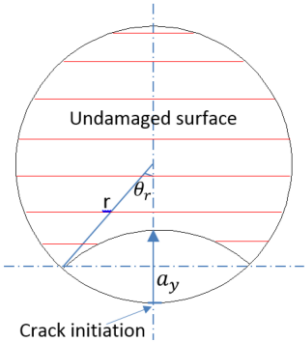

Figure 3.0: crack growth on a reinforcing bar cross section [15]

4 FINITE ELEMENT IMPLEMENTATION

Stresses are generally related to strains as shown in the following equation:

$$\{\sigma\} = [D]\{\varepsilon\} \quad (19)$$

where in 2-D (Figure 4.0),

$$\{\sigma\} = \begin{bmatrix} \sigma_x \\ \sigma_y \\ \tau_{xy} \end{bmatrix} \text{ and} \quad (20)$$

$$\{\varepsilon\} = \begin{bmatrix} \varepsilon_x \\ \varepsilon_y \\ \gamma_{xy} \end{bmatrix} \quad (21)$$

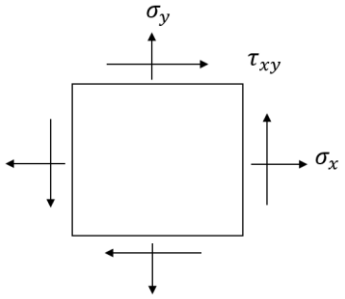

Figure 4.0: Stresses acting on a reinforced concrete panel element.

$$[D] = [D_c] + \sum [D_s]_i \quad (22)$$

$$[D_c] = [T_c]^T [D_c]' [T_c] \quad (23)$$

$$[D_c]' = \begin{bmatrix} \bar{E}_{c1} & 0 & 0 \\ 0 & \bar{E}_{c2} & 0 \\ 0 & 0 & \bar{G}_{c1} \end{bmatrix} \quad (24)$$

$$[D_s]_i = \begin{bmatrix} \rho_i \bar{E}_{si} & 0 & 0 \\ 0 & 0 & 0 \\ 0 & 0 & 0 \end{bmatrix} \quad (25)$$

For concrete,

$$\{\varepsilon\} = \{\varepsilon_c\} + \{\varepsilon_c^{fat}\} \quad (26)$$

where
$\{\varepsilon\}$ is the total element strains.
$\{\varepsilon_c\}$ is the concrete net elastic strains.
$\{\varepsilon_c^{fat}\}$ is the fatigue prestrain for concrete.

It is important to emphasize that other prestrains such as creep, Alkaline Aggregate Reaction strains, and slip derived from Equation 14 based on The DSFM Theory, may be included in Equation 26.

For reinforcement,

$$\{\varepsilon\} = \{\varepsilon_s\}_i + \{\varepsilon_s^{fat}\} \quad (27)$$

$\{\varepsilon\}$ is the total element strains.
$\{\varepsilon_s\}_i$ is the reinforcement net strains.
$\{\varepsilon_s^{fat}\}$ is the fatigue prestrain for steel (other reinforcement prestrains may be added).

From these equations, the compressive stiffness and the tensile stiffness in concrete and the tensile stiffness in steel reinforcement can be written thus:

$$\bar{E}_{c2} = \frac{f_{c2}}{(\varepsilon_{c2} - \varepsilon_{c2}^{fat})} \quad (28)$$

$$\bar{E}_{c1} = \frac{f_{c1}}{(\varepsilon_{c1} - \varepsilon_{c1}^{fat})} \quad (29)$$

$$\bar{E}_{si} = \frac{f_{si}}{(\varepsilon_i - \varepsilon_{si}^{fat})} \quad (30)$$

ε_i is obtained from the total strain in the ith direction.

The constitutive relation for concrete and steel reinforcement can be written as:

$$\{\sigma\} = [D]\{\varepsilon\} - \{\sigma^0\} \quad (31)$$

$$\{\sigma^0\} = [D_c]\left(\{\varepsilon_c^{fat}\}\right) + \sum_{i=1}^{n} [D_s]_i \left(\{\varepsilon_s^{fat}\}_i\right) \quad (32)$$

Since the fatigue prestrains for concrete are in the principal direction, the prestrains may need to be transformed back to x, y axes. Hence

$$\varepsilon_{cx}^{fat} = \frac{1}{2}\varepsilon_{c1}^{fat}(1 + \cos 2\theta) + \frac{1}{2}\varepsilon_{c2}^{fat}(1 - \cos 2\theta) \quad (33)$$

$$\varepsilon_{cy}^{fat} = \frac{1}{2}\varepsilon_{c1}^{fat}(1 - \cos 2\theta) + \frac{1}{2}\varepsilon_{c2}^{fat}(1 + \cos 2\theta) \quad (34)$$

$$\gamma_{cxy}^{fat} = \varepsilon_{c1}^{fat} \sin 2\theta - \varepsilon_{c2}^{fat} \sin 2\theta \quad (35)$$

The solution to these sets of equations is iterative and a full description of the algorithm may be found in [9 and 10]. It is worth indicating that the bond behaviour between concrete and steel is accounted for in the MCFT/DSFM algorithms.

5 CORROBORATION RESULTS

Experimental results from [16] were employed to validate the proposed fatigue damage analysis approach in this paper. The test set up is shown in Figure 5.0. Table 1 presents the properties of the specimens under consideration. The reinforced concrete beams used in the experiments had dimensions of 700 mm x 250 mm x 180 mm.

Material properties obtained from the tests in [15] include a compressive strength of 59 MPa, tensile strength of 2.03 MPa, cylinder strain at peak strength of 2.03 x 10^{-3}, and a maximum aggregate size of 10 mm. The bottom reinforcement consisted of two different diameters: 10M rebars (Canadian standard) labeled as C, and 15M rebars (Canadian standard) labeled as C'.

D4 rebars (Canadian standard) were used as shear reinforcement (0.2%). The average yield strengths for the 15M, 10M, and D4 bars were 430 MPa, 480 MPa, and 610 MPa, respectively, with ultimate strengths reported as 700 MPa, 600 MPa, and 630 MPa.

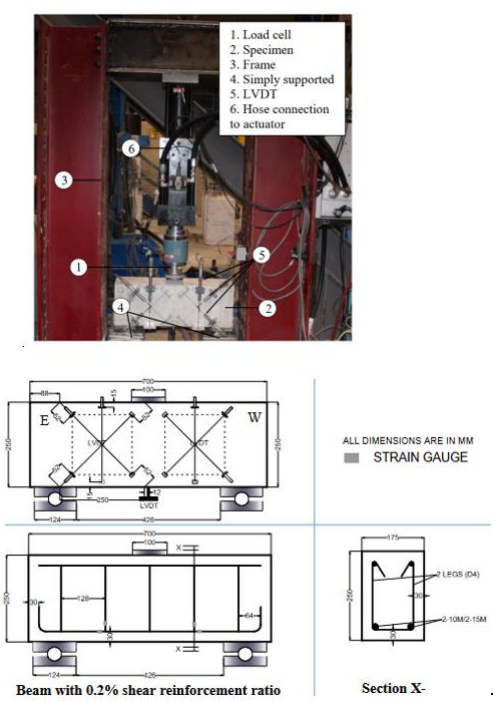

Figure 5.0: Test set-up

The capacities for Beams C and C' were 270 kN and 390 kN, respectively (see Figure 6.0). In the fatigue testing, loading was applied at 70% and 80% of the capacities of Beams C and C', respectively, on four beams, as shown in Table 1.0. In each case, the minimum load was 5 kN.

Verification analyses were performed using the VecTor2 nonlinear analysis software, yielding monotonic capacities of 250 kN and 350 kN for Beams C and C', respectively. For the fatigue analysis in VecTor2, 70% and 80% of the static strengths were used. The results of the analyses are summarized subsequently.

Table 1.0: Specimens description and experiment results

ID	f_c (MPa)	ρ_l%	ρ_v%	Max. fat. load (%P_u)	Min. fat. Load (%P_u)	N_f x 10^3
C		0.45	0.2	Mono.	-	-
C’		0.9	0.2	Mono.	-	-
C80		0.45	0.2	80	1.8	47
C70		0.45	0.2	70	1.8	72
C’80		0.9	0.2	80	1.3	62
C’70		0.9	0.2	70	1.3	190

ρ_l% : longitudinal reinforcement ratio;
ρ_v%: shear reinforcement ratio; P_u is the beam monotonic capacity.

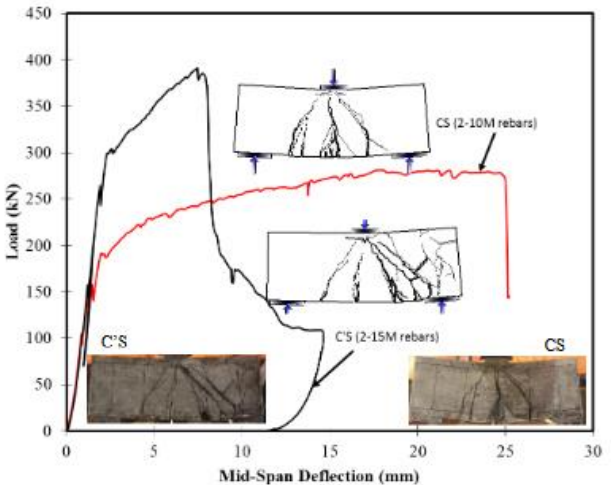

Figure 6.0: Monotonic loading results from experiment (no correction for frame settlement).

Figure 7.0 illustrates the results of the monotonic loading analysis. The obtained profiles closely resemble those observed in the experiments, and the load-deformation profiles of Beam C and Beam C' display flexural and shear-critical responses, consistent with the experimental results.

The fatigue analysis results for the four beams are presented in Figure 8.0. Figure 9.0 provides a comprehensive comparison between the finite element analysis and the experimental results, showcasing a favorable agreement between the two.

Figure 10.0 presents the post-failure condition of Beam C80. Notably, the failure occurred due to the fracturing of the longitudinal reinforcement, while none of the stirrups ruptured. The crack pattern observed in the analysis aligns with the experimental results, further validating the accuracy of the analytical approach.

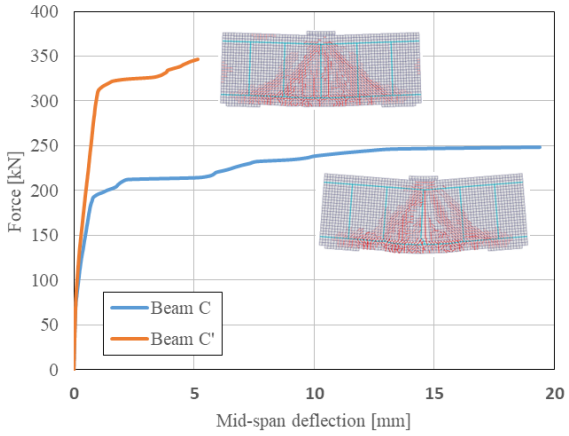

Figure 7.0: Monotonic loading results from finite element analysis

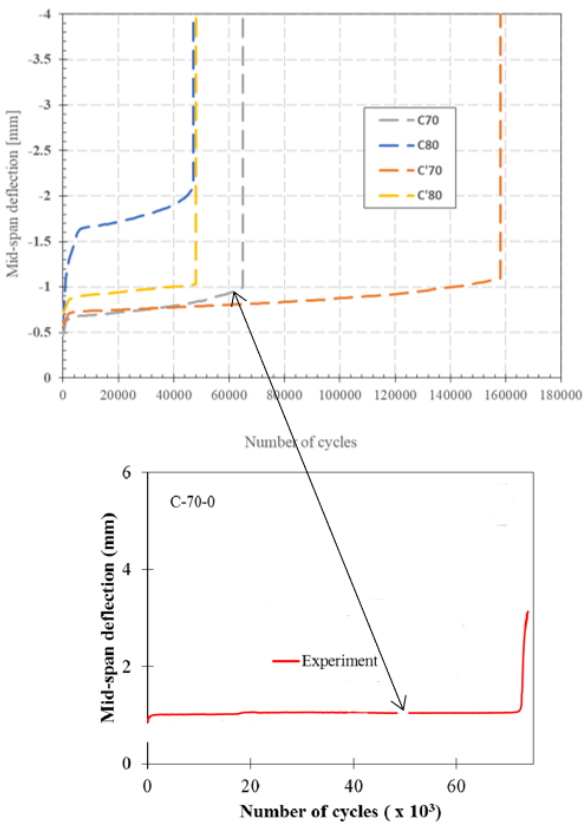

Figure 8.0: Mid-span deflection versus number of fatigue loading cycles (FEA and experiment)

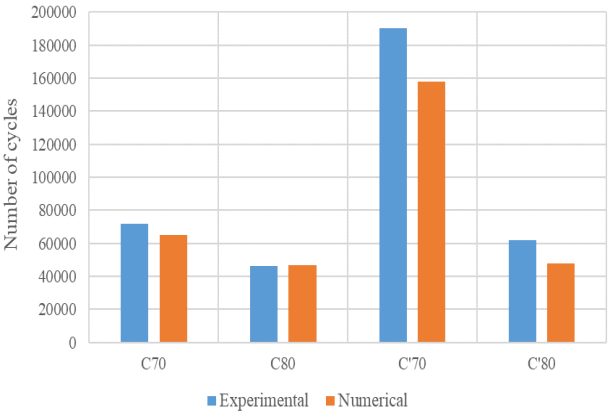

Figure 9.0: Comparison of results from finite element analysis and experiment

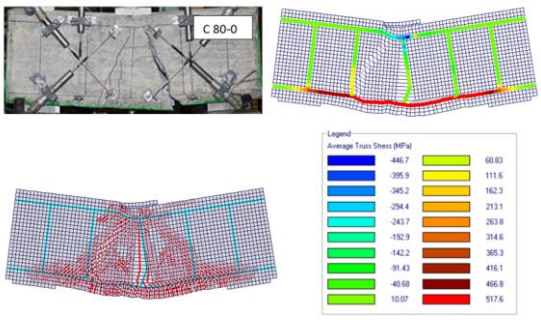

Figure 10.0: Fatigue damage patterns from finite element analysis before Beam C80 rupture.

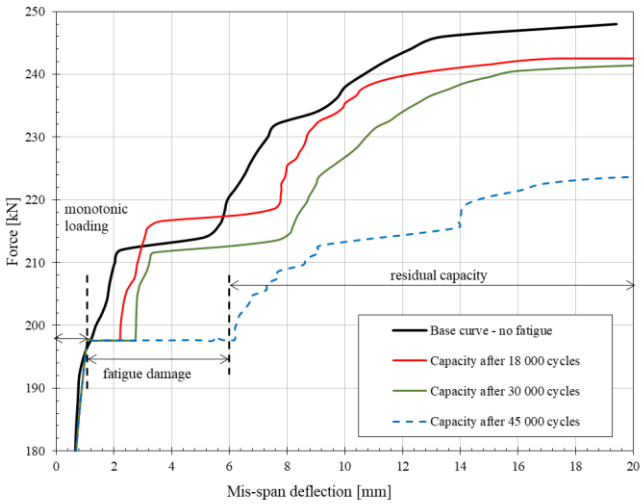

Figure 11.0: Residual capacity of Beam C80 after fatigue loading of 45 000 cycles.

6 CONCLUSIONS

As emphasized in the introductory section, stress-life models are primarily applicable during the design stage. However, for fatigue-prone structures subjected to abnormal loading, environmental degradation, or chemical reactions, determining the residual capacity during service becomes crucial for making critical decisions to prevent catastrophic failures.

Figure 11 illustrates the residual capacity of Beam C-80-0 after 18,000 cycles, 30,000 cycles, and after 45,000 cycles (approaching failure). Considering the load-deformation curve after 45,000 cycles, three regions are obvious. The first region shows an increase of load from zero to the fatigue load (197.6 kN). The second region consists of an increasing deformation at a constant load (fatigue load). The third region shows the residual capacity of the beam after the fatigue loading.

It can be inferred from the figure that the failure of the beam will occur when the residual capacity becomes equal to the applied load. This can be observed in Figure 8.0 as 47,000 cycles.

Since fatigue loads on fatigue-prone structures such as wind turbines are routinely recorded, the reactions on the reinforced concrete structural elements can be calculated. By incorporating the number of loading cycles, the proposed analysis approach may be used to estimate the residual capacity of these structures after years of service.

The approach presented in this study primarily focuses on two-dimensional analysis. However, efforts are currently underway to implement the models into a three-dimensional Finite Element Analysis (FEA) algorithm. This advancement aims to enable comprehensive analysis of structures that require three-dimensional modeling to accurately capture their behavior and response under real-world operational conditions.

REFERENCES

[1] Fib Model Code 2010. (2013). *"FIB Model Code for Concrete Structures* – FIB-Federation.

[2] American Concrete Institute 215. *Concrete Design for Fatigue Loading- Report*. PREC-215-21.

[3] CSA S6. Canadian Highway Bridge Design Code. CSA S6:19.

[4] BSI, Eurocode 2: *Design of Concrete Structures* (EN1992-1-1). (2005).

[5] Dongyun, L., Chao. W., Jamie. G., Tong. G., Jie. C., Yongming. T., Lennart. E., Gabriel. S., 2023. *A Review of Concrete Properties under the Combined Effect of Fatigue and Corrosion from a Material Perspective.* Construction and Building Materials, Vol. 369, 130489.

[6] Isojeh, B., El-Zeghayar, M., and Vecchio, F.J. (2017). *Simplified Constitutive Model for Fatigue Behaviour of Concrete in Compression.* Journal of Materials in Civil Engineering,DOI: 10.1061/(ASCE)MT.1943-5533.0001863

[7] Isojeh, B., El-Zeghayar, M., and Vecchio, F.J. (2017a). *Concrete Damage under Fatigue Loading in Uniaxial Compression.* ACI Materials Journal, Vol. 114, No. 2, pp. 225-235.

[8] Zhang B., Phillips D.V., and Wu K. (1996). "Effects of Loading Frequency and Stress Reversal on Fatigue Life of Plain Concrete." Magazine of Concrete Research, Vol. 48, pp. 361-375.

[9] Vecchio, F.J. (2000). *Disturbed Stress Field Model for Reinforced Concrete: Formulation.* Journal of Structural Engineering, Vol. 126, No. 8, pp. 1070-1077.

[10] Vecchio, F.J. (2001). *Disturbed Stress Field Model for Reinforced Concrete: Verification.* Journal of Structural Engineering, Vol. 127, No. 1, pp. 1070-1077.

[11] Lee, S.C., Cho, J.Y., Vecchio, F.J. (2016). *Analysis of Steel Fibre-Reinforced Concrete Elements Subjected to Shear*. ACI Structural Jorunal, Vol. 113, No. 2, pp. 275-285.

[12] Isojeh, M.B., Vecchio, F.J. (2016). *Parametric Damage of Concrete under High-Cycle Fatigue Loading in Compression*. Proc., 9th International Conference on Fracture Mechanics of Concrete and Concrete Structures., FraMCoS-9.

[13] Isojeh, B., El-Zeghayar, M., and Vecchio, F.J. (2017a). *High-Cycle Fatigue Life Prediction of Reinforced Concrete Deep Beams.* Engineering Structures Journal, Vol. 150, pp. 12-24.

[14] British Standard (2005). *Guide to Methods for Assessing the Acceptability of Flaws in Metallic Structures.* BS 7510.

[15] Total Materia (2010). *Linear Elastic Fracture Mechanics (LEFM): Part Two*: Total Materia Article

[16] Isojeh, B., El-Zeghayar, M., and Vecchio, F.J. (2017). *Numerical Analysis of Reinforced Concrete and Steel-Fiber Concrete Elements under Fatigue Loading*. Journal of Structural Engineering, Vol. 145, No. 11.